Oral Presentation

The 7th TSME International Conference on Mechanical Engineering
13-16 December 201

TSME ICOME 2016
Mechanical Engineering Innovation for Green Society

TSF0025

Visualization of Diverse Flows between Co-Rotating Disks in Casing by Numerical Analysis and Experiment

Ryosuke Uenishi[1,*], Shouhei Tsugawa[1], Tyuyoshi Maeda[1], Morihiko Uesaka[2], Takashi Watanabe[2], Hirochika Tanigawa[3] and Katsuya Hirata[1]

[1] Department of Mechanical Engineering, Doshisha University, Kyoto, 610-0321, Japan
[2] Department of Information Science, Nagoya University, Nagoya, 464-8601, Japan
[3] Department of Mechanical Engineering, NIT Maizuru College, Maizuru, 625-0016, Japan
[*] Corresponding Author: duq0575@mail4.doshisha.ac.jp, +81-(0)774-65-7746, +81-(0)774-15-6830

Abstract

The authors experimentally and numerically investigate the flow between co-rotating disks, namely, which rotate co-axially in the same direction at the same angular velocity, with a narrow gap enclosed by a stationary shroud at their circumferences. The flow often accompanies azimuthally-fluctuating instabilities; a non-axisymmetric secondary flow near the shroud. The authors focus upon the flow in torus-vortex modes, in addition to core-shape modes. Specifically, in experiments, the authors visualize the meridian plane (r-θ plane) and the midplane (r-z plane) between co-rotating disks, by using a high-speed video camera and a YAG laser to carry out particle-image-velocimetry (PIV) analysis. Based on such PIV results, the torus-vortex modes and the core-shape modes are defined. By numerical calculations, the authors reveal the details of diverse flow structures in those modes.

Keywords: Rotating Disks, Rotating Flow, Numerical Calculation, Flow Visualization, PIV Analysis

1. Introduction

The flow in the neighborhood of a rotating disk gives a practical importance, particularly in connection with rotary machines (Schlichting, 1979 [1]) common in turbo-machineries. First, the flow on a single infinite rotating disk or the flow between two infinite co-axially rotating disks has been studied by many researchers [2, 6]. Then, the flow around a single and shrouded rotating disks with a finite radius and the flow between two finite co-axial rotating disks have been studied as well [7, 11]. These flow problems can be found out in various fundamental industrial applications such as axial compressors, vane less diffusers, multiple-disk pumps and disk/drum-brake systems. In general, these types of flow tend to include non-axisymmetric secondary flows known as 'stall propagations' which occasionally cause disk vibrations and noises [12, 15].

Now, we consider the flow between two co-rotating disks, which rotate co-axially in the same direction at the same angular velocity and have a narrow gap enclosed by a stationary shroud at their circumferences. The flow is modelled on that inside the random-access disk storage devices of computers. The flow has been studied by many researchers [16, 28], because, the flow is very complicated with three-dimensionality and turbulence. For example, when we visualize the flow in the midplane (r-θ plane) between disks, we often see an azimuthally-fluctuating instability which exhibits a non-axisymmetric secondary flow near the shroud with a clear boundary. The boundary exists between the core region which is the laminar-flow region around the center hub and the outer region where the flow is turbulent. The boundary between the core region and the outer region has a near-polygonal shape, such as hexagon, pentagon, square, triangle and ellipse, together with circle. The core-boundary shape rotates at a slightly slower than the disks, while the fluid in the core region rotates with the disks. On the other hand, when we visualize the flow in the meridional plane (r-z plane) between the disks, we often see a pair of torus-vortex structures near the shroud.

On the basis of the core-boundary shape, the authors have classified these instability flows into six modes as a function of the Reynolds number Re and three geometric parameters λ, δ and κ (Hirata et al., 2006 [24]). Hereinafter, the modes are referred to core-shape modes CSMs. We have revealed the stability diagrams concerning CSMs of the flow (Hirata et al., 2011 [25]). Recently, we conduct numerical analysis on the flow (Arimitsu et al., 2013 [27]) and experiment on flow visualization (Tsugawa et al., 2015[28]).

In the present study, we experimentally and numerically research the flow in other modes called torus-vortex modes TVMs, in addition to CSMs. Especially in numerical calculations, we compare computational results with experiment results, and try to reveal the details of flow structures in each mode.

2. Methodology

2.1 Flow Model and Governing Parameters

Fig. 1 shows a side view of the present model. The model is composed of two coaxial rotating disks and a stationary peripheral shroud assembled from two annuli and a cylinder. The disks rotate in the same direction at the same angular velocity Ω_d with a narrow spacing G.

In the present study, as non-dimensional system parameters, we can choose a disk-tip Reynolds number $Re \equiv \Omega_d R_d^2/\nu$, a gap aspect ratio $\delta \equiv G/R_d$, a non-dimensional peripheral radius $\lambda \equiv R_w/R_d$ and non-dimensional hub radius $\kappa \equiv R_h/R_d$, where R_d, R_w and R_h are the radii of the rotating disk, the cylindrical shroud wall and the hub, respectively. ν denotes the kinematic viscosity of the fluid. Characteristic velocity is the disk-tip velocity $R_d\Omega_d$. Such four parameters as Re, δ, λ and κ are the most sensitive ones for the present phenomenon in concern.

Tables 1 and 2 summarize the experimental and computational parameters, respectively. In the experiment, the value of λ is 1.01 and the flow model has an inevitable radial clearance between the disk tip and the shroud wall. Though some influences of this clearance may be found very close to the shroud, we follow our supplemental experiments and conclude that the effect on the whole flow structure is negligible.

Table 1 Experimental parameters.

Disk-tip Reynolds number Re ($\equiv \Omega_d R_d^2/\nu$)	$1.4\times10^3 - 1.4\times10^5$
Gap aspect ratio δ ($\equiv G/R_d$)	0.10 – 0.30
Non-dimensional enclosure radius λ ($\equiv R_w/R_d$)	1.01
Non-dimensional hub radius κ ($\equiv R_h/R_d$)	0.11, 0.20, 0.50

Table 2 Computational parameters.

Disk-tip Reynolds number Re ($\equiv \Omega_d R_d^2/\nu$)	$1.4\times10^3 - 1.4\times10^4$
Gap aspect ratio δ ($\equiv G/R_d$)	0.10 – 0.30
Non-dimensional enclosure radius λ ($\equiv R_w/R_d$)	1.0
Non-dimensional hub radius κ ($\equiv R_h/R_d$)	0.11

2.2 Experiment

In experiments, we attempt to visualize the midplane (r-θ plane) and the meridional plane (r-z plane) between the co-rotating disks by using a high-speed video camera and a YAG laser to carry out particle-image-velocimetry (PIV) analysis.

Fig. 2 shows a schematic diagram of the present experimental apparatus. Two acrylic disks are submerged in a cylindrical wall. For flow visualizations, the upper disk and cylindrical wall are transparent and the others are frosted. The flow between the disks is visualized using suspended polyethylene or SiO_2 particles, and it is recorded by a high-speed video camera over the disks. In the top view, the disks rotate clockwise at an angular velocity Ω_d by a variable-speed drive motor located underneath the tank. The angular velocity Ω_d is monitored by a rotary encoder linked with the rotating shaft. The details of experimental method can be found in our previous studies [27, 28]. Reversed rotation of the disks gives the same result. This show the accuracy of present experimental setup.

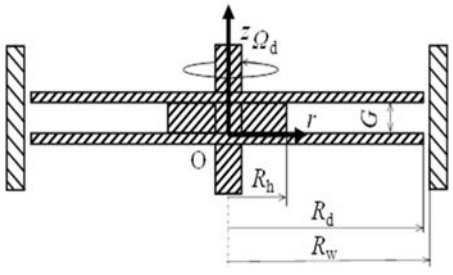

G : Gap
R_d : Radius of rotating disk (= 153 mm)
R_h : Radius of hub
R_w : Radius to stationary outer wall (= 155 mm)
Ω_d : Angular velocity of disk rotation, $= 2\pi/T_d$
(Ω_c : Angular velocity of core shape)

Fig. 1 Model, together with experimental parameters and coordinate system

2.3 Numerical Analysis

We assume that Mach number M is much smaller than unity. Therefore, fluid is supposed to be incompressible. So, the governing equations are the incompressible unsteady Navier-Stokes equations and the equation of continuity.

These equations in a cylindrical coordinate system are solved by a finite difference method based on the MAC method [29] with the FTCS scheme using a staggered grid system. We use the Poisson equation for p instead of the equation of continuity. We carry out some preliminary computations before main computations in order to confirm numerical accuracy, and tune up the grid size, the time step and so on. Fig. 3 shows the present computational grid. The grid is a staggered one with non-equivalent spacing. The details of grid, boundary condition and so on, can be found in our previous study [27].

3. Results and Discussion

3.1 Core-shape mode

In this subsection, we discuss the core-shape mode CSM, obtained from the experimental and numerical results. To conclude, we will classify the concerning flows into some CSMs, and show the stability diagram of CSMs.

By flow experiments, we have confirmed a distinct boundary between the inner region near the central hub and the outer region near the shroud, as had been shown by Lennemann [16]. The boundary geometry shape called the core shape depends on system parameters. By flow visualizations with PIV analysis, we can see that

there exists a distinct boundary between the inner region around the central axis where vorticity ζ_z is almost twice of the disk-rotation speed Ω_d, where ζ_z is non-dimensional axial vorticity, and the outer region near the shroud where the turbulent flow is dominant with small and perturbed vorticity. This confirms the rigid-rotation motion in the core area.

We can also confirm that the core boundary has a nearly-polygonal configuration, and that the configuration rotates at an angular speed Ω_c which is slightly lower than the disk-rotation speed Ω_d. In this case, the potential flow theory (the Kelvin's theorem) is applicable to Ω_c [24]. For further discussion, we define the circumferential flow mode corresponding to the number of polygonal vertices. As shown in Fig. 4, we identified six different core-shape modes in accordance with the modal number m: circular for $m = \infty$(panels (a) and (b)), hexagonal for $m = 6$(panel (c)), pentagonal for $m = 5$ (panel (d)), square for $m = 4$(panel (e)), triangular for $m = 3$(panel (f)), and elliptical for $m = 2$(panel (g)). The core-shape mode ∞ means an almost circular boundary at any instants. Note that, by flow visualizations, identification of modes more than 6 is possible but tends to be affected by observer's bias. Hereinafter, we refer to the core-

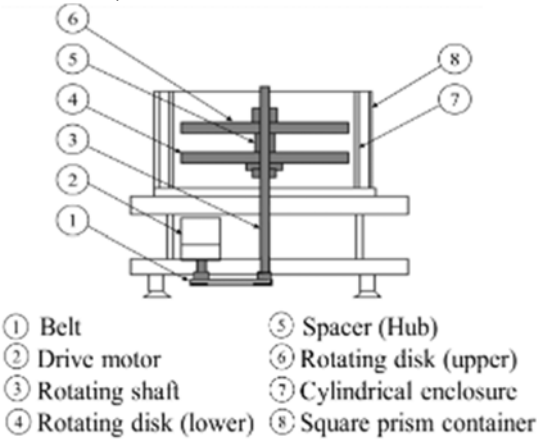

Fig. 2 Schematic diagram of experimental apparatus.

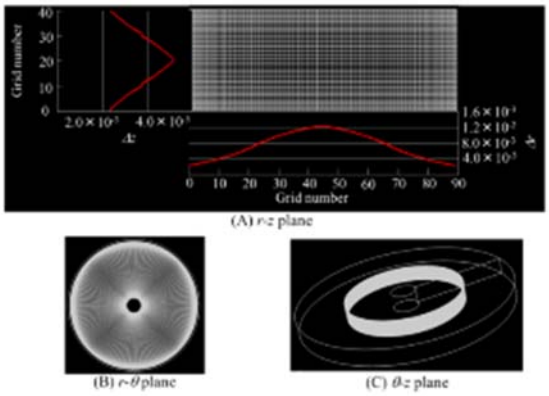

Fig. 3 Grid for computation ($GN_r \times GN_\theta \times GN_z$ = 90×120×40, $\delta = 0.15$, $\lambda = 1.0$ and $\kappa = 0.11$).

shape modes ∞, 6, 5, 4, 3, and 2 as CSM ∞, CSM 6, CSM 5 CSM 4, CSM 3 and CSM 2, respectively.

We successfully identify these six CSMs by both experiment and numerical analysis. Those modes will be visualized in Subsection 3.3.

3.2 Torus-vortex mode

In the preceding subsection, we have discussed the core-shape modes CSMs obtained by the flow visualization on the r-θ plane. In this subsection, we conduct the flow visualization on the r-z plane (the meridional plane). As a result, we have revealed six torus-vortex modes TVMs: TVM 1, TVM 1A, TVM 1B, TVM 2, TVM 2B and TVM 3. In addition to CSM, TVM is the another definition of instability of the flow in concern.

In TVM 1, the torus vortices are steady and symmetric about the midplane between disks. On the other hand, in TVM 1A, the torus vortices cyclically repeat the expansion and the contraction with a certain period mainly in the axial direction. In TVM 1B, the torus vortices cyclically repeat the expansion and the contraction as well as TVM 1A. However, the amplitude of the expansion/contraction is much larger than TVM 1A. That is, the amplitude is distinctive in the radial direction in addition to the axial direction. In TVM 2, the torus vortices are almost steady and axisymmetric, though the symmetry about the midplane is obviously broken. It should be noted that the upper torus vortex is larger than the lower one. However, which of the torus vortices is larger depends upon to hysteresis. In TVM 2B, the torus vortices are non-axisymmetric unlike TVM 2. The torus vortices are not almost steady but periodically fluctuate, in both the axial and radial directions. In TVM 3 that is not found by numerical analysis, it is difficult to confirm the torus vortices. Fluctuating manner of the flow is not periodic, but rather random.

Again, we successfully identify these six TVMs by both experiment and numerical analysis. Those modes will be visualized in Subsection 3.3.

Now, we show the stability diagram concerning the torus-vortex modes TVMs together with the core-shape modes CSMs, at $\kappa = 0.11$ in wide ranges of other two system parameters of the disk-tip Reynolds number Re and gap aspect ratio δ. Fig. 5 summarizes all the experimental results. Green regions denote CSMs. Red solid lines denote the border between TVMs stable regions. For reference, brown lines, blue lines and black lines denote the results by Abrahamson *et al*. (1989) [17], Herrero *et al*. (1999) [22] and Randriamampianina *et al*. (2001) [23], respectively.

About CSMs, the increases of Re and δ tend to decrease the modal number of CSM. About TVMs, the increases of Re and δ is apt to enhance the irregularity of the TVM (axisymmetry, unsteadiness and aperiodicity), while the process reaching the irregularity is complex. The increase of δ influences the asymmetry of TVM 1 and TVM 2. The increase of the Re promotes the non-axisymmetry of TVM 2 and TVM 2B, the

aperiodicity of TVM 3 and the amplitude of the periodic oscillation of TVM 1A, TVM 1B and TVM 2B. The parameter δ has the influences similar to that of Re. These influences are not found in the previous studies to the authors' knowledge, and they are one of the primary facts found in the present investigation.

Fig. 6 shows the comparison between the numerical result and the experimental result on the stability diagram of CSMs and TVMs for λ =1.0 and κ = 0.11. The number above each symbol denotes the modal number of CSM. Blue solid lines denote the border between TVMs stable regions. The Green regions and the red solid lines are the same as those in Fig. 5. We can see good agreement between the experimental and the numerical results concerning both CSM and TVM.

3.3 Flow structure

Numerical analysis is useful to investigate the concerning flow in detail. In general, it is difficult to estimate numerical accuracy for non-linear phenomena such as the cornering flow. However, we have confirmed it by the comparison with experimental results.

In order to examine three dimensional structure of the concerning flow, we visualize the flow to use second invariant of velocity gradient tensor Q and non-dimensional circumferential vorticity component ζ_θ and axial vorticity component ζ_z. We normalize these quantities using R_d and Ω_d.

Figs. 7-13 show some examples obtained by numerical analysis to visualize the whole three-dimensional structures of the concerning flows in the models at an instant from a comprehensive point of view. In each figure, panel (a), (b), (c), (d) and (e) denote the iso-surfaces with certain values of Q = 0.75-4.0, $|\zeta_\theta|$ = 1.5-4.5, $|\zeta_z|$ = 0.2-1.3, ζ_z = 0 and ζ_z = 1.87-1.95, respectively.

At first, Fig. 7 exhibits the flow at $Re = 1.4\times10^3$, δ = 0.10, λ =1.0 and κ = 0.11. The flow is in CSM ∞ and TVM 1. Panel (a) well corresponds to both perfect axisymmetry and steadiness of the flow. A clear axisymmetric pair of the torus vortices is observed in panel (b) and a circular central core in the rigid rotation with disks is found in panel (e).

Second, Fig 8 presents the flow at $Re = 2.7\times10^3$, δ = 0.30, λ =1.0 and κ = 0.11. The flow is in CSM ∞ and TVM 2. Again, panel (a) well corresponds to both perfect axisymmetry and steadiness of the flow. A clear non-symmetric pair of the torus vortices appears in panel (b) and a circular central core in the rigid rotation with disks is found in panel (e).

Thirdly, Fig. 9 represents the flow at $Re = 4.1\times10^3$, δ = 0.15, λ =1.0 and κ = 0.11. The flow is in CSM ∞ and TVM 1A. Panel (a) well corresponds to the flow with a periodic fluctuation, which is related spatially-periodic with the rotating flow structure in the outer region known as the shift-and-reflect symmetry (Herero et al. [22]). A clear axisymmetric

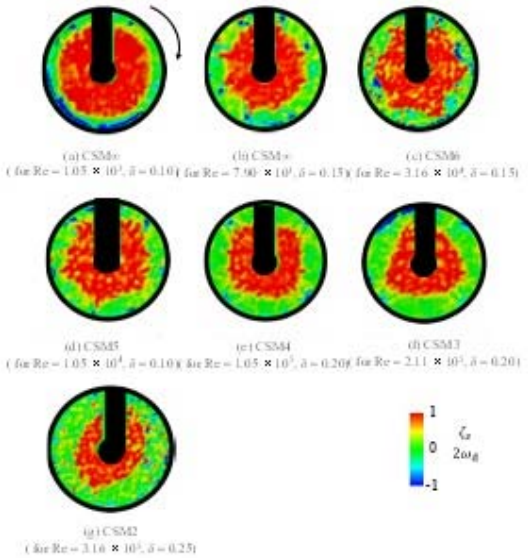

Fig. 4 Distributions of vorticity ζ_z on the midplane between disks (on the r-θ plane at z/G = 0.5), together with velocity vectors (for λ = 1.0 and κ = 0.11 by experiment).

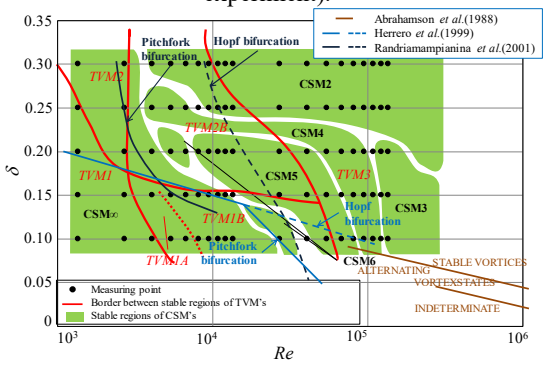

Fig. 5 Stability diagram of torus-vortex modes TVM 1 – TVM 3, in addition to that of core-shape modes CSM ∞ ― CSM 2 for λ = 1.0 and κ = 0.11, experimental result.
(Green regions denote the stable ones of CSMs.)

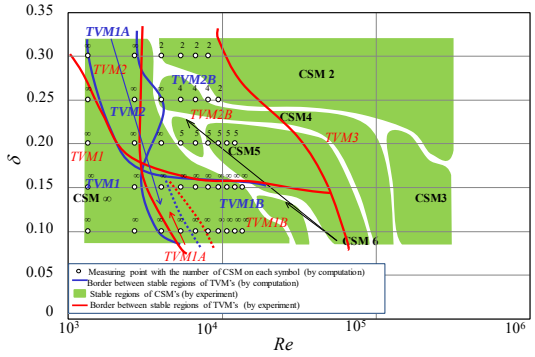

Fig. 6 Comparison between numerical and experimental results on stability diagram of core-shape modes CSM ∞ – CSM 2, together with these of torus-vortex modes TVM 1 – TVM 3 for λ = 1.0 and κ = 0.11.

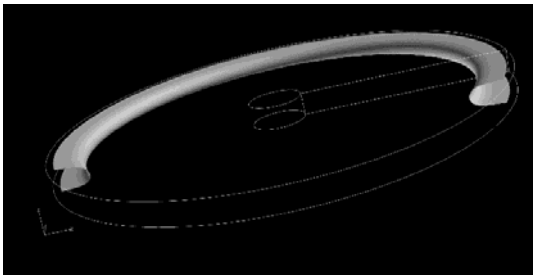

(a) $Q = 0.75$

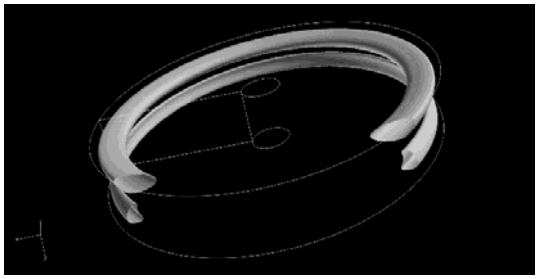

(a) $Q = 1.50$

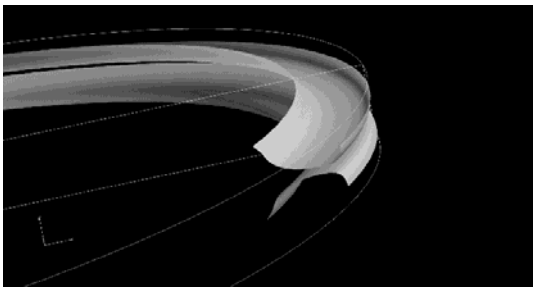

(b) $|\zeta_\theta| = 1.40$

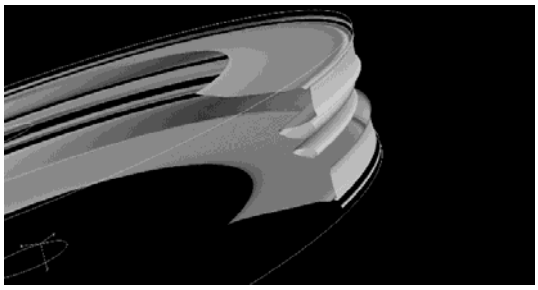

(b) $|\zeta_\theta| = 2.90$

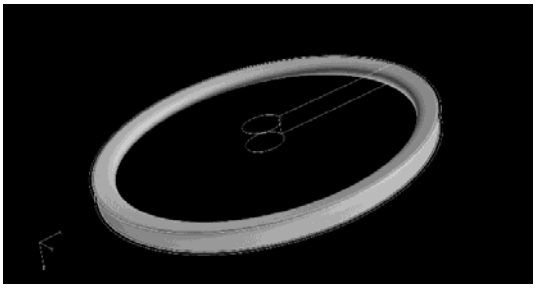

(c) $|\zeta_z| = 0.96$

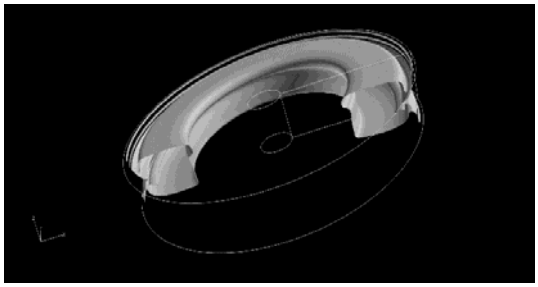

(c) $|\zeta_z| = 1.30$

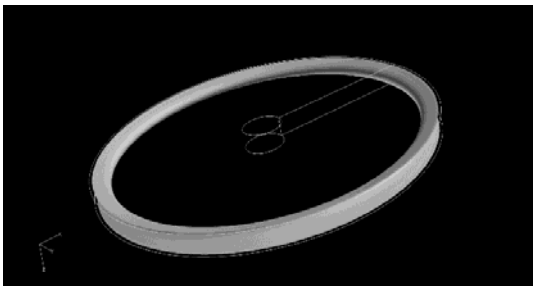

(d) $\zeta_z = 0$

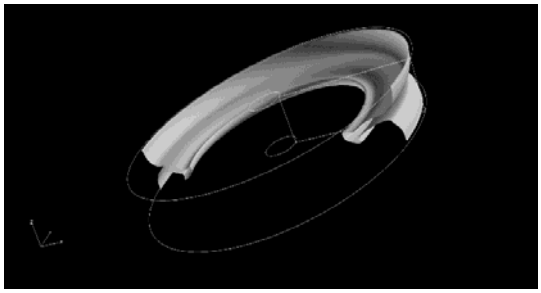

(d) $\zeta_z = 0$

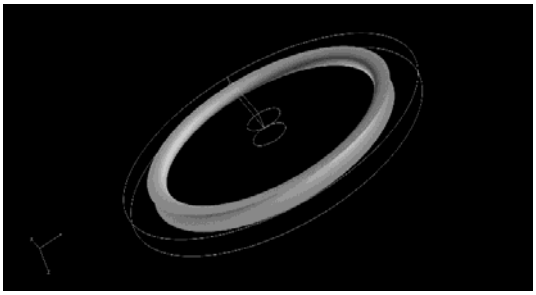

(e) $\zeta_z = 1.95$

Fig. 7 Iso surfaces at an instant in CSM ∞ and TVM 1 at $Re = 1.4\times10^3$, $\delta = 0.10$, $\lambda = 1.0$ and $\kappa = 0.11$

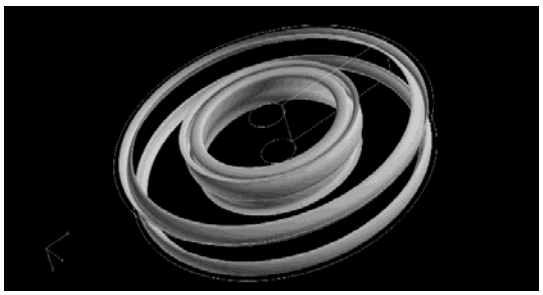

(e) $\zeta_z = 1.95$

Fig. 8 Iso surfaces at an instant in CSM ∞ and TVM 2 at $Re = 2.7\times10^3$, $\delta = 0.30$, $\lambda = 1.0$ and $\kappa = 0.11$

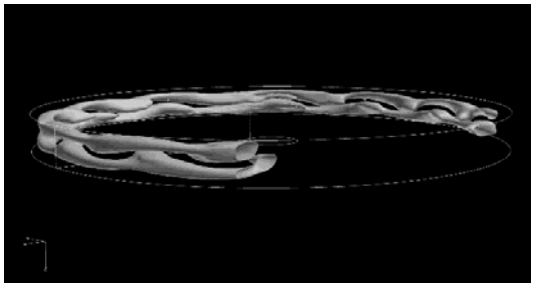

(a) $Q = 2$

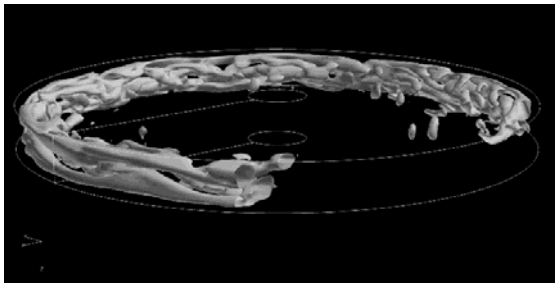

(a) $Q = 2$

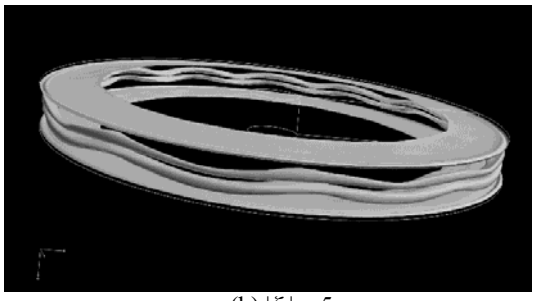

(b) $|\zeta_\theta| = 5$

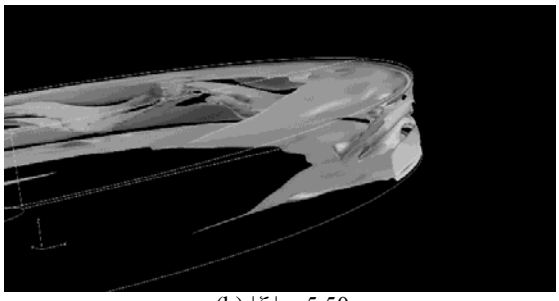

(b) $|\zeta_\theta| = 5.50$

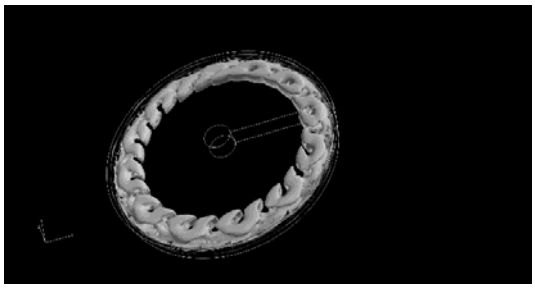

(c) $|\zeta_z| = 0.55$

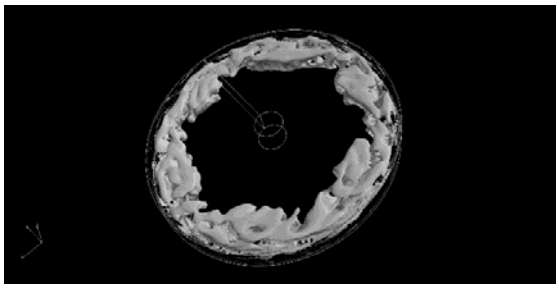

(c) $|\zeta_z| = 0.62$

(d) $\zeta_z = 0$

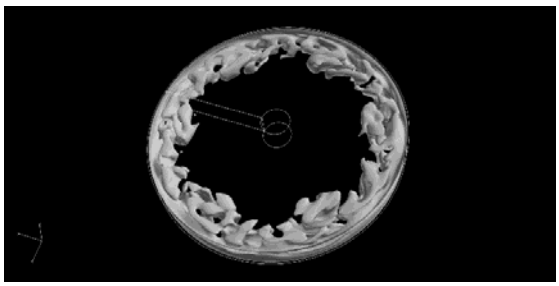

(d) $\zeta_z = 0$

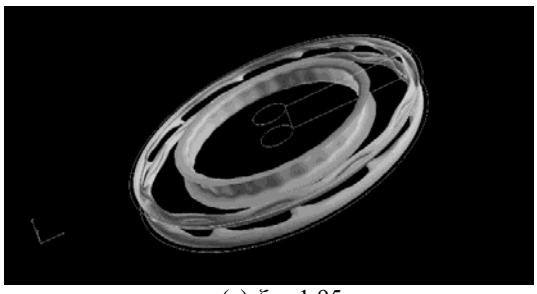

(e) $\zeta_z = 1.95$

Fig. 9 Iso surfaces at an instant in CSM ∞ and TVM 1A at $Re = 4.1\times10^3$, $\delta = 0.15$, $\lambda = 1.0$ and $\kappa = 0.11$

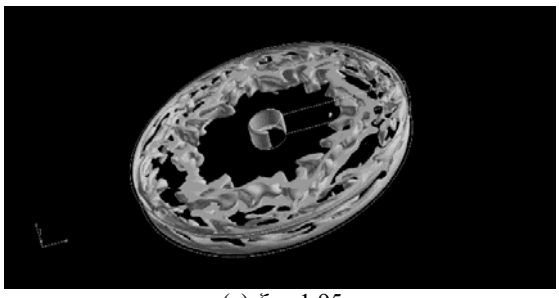

(e) $\zeta_z = 1.95$

Fig. 10 Iso surfaces at an instant in CSM 6 and TVM 1B at $Re = 8.2\times10^3$, $\delta = 0.15$, $\lambda = 1.0$ and $\kappa = 0.11$

TSF0025

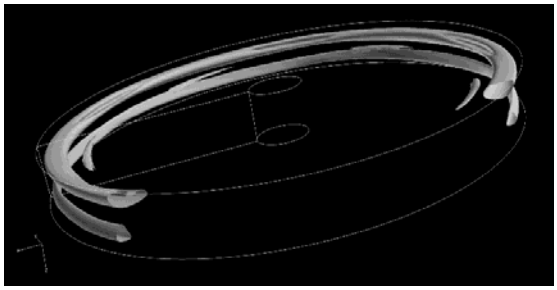

(a) $Q = 4$

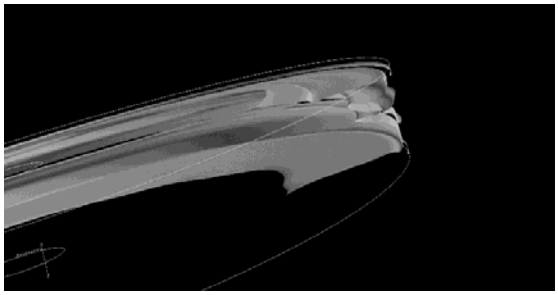

(b) $|\zeta_\theta| = 3.50$

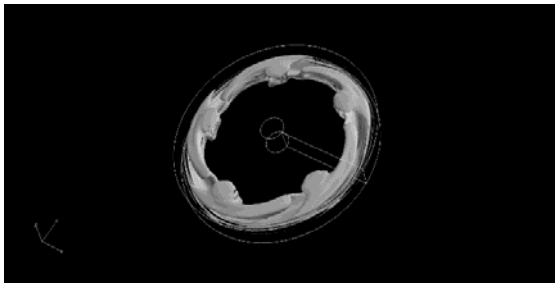

(c) $|\zeta_z| = 0.26$

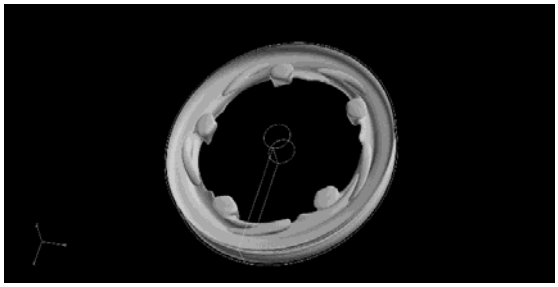

(d) $\zeta_z = 0$

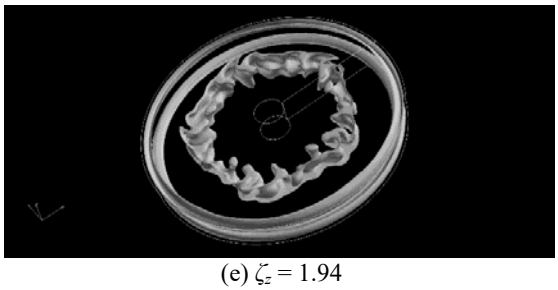

(e) $\zeta_z = 1.94$

Fig. 11 Iso surfaces at an instant in CSM 5 and TVM 2B at $Re = 5.4\times10^3$, $\delta = 0.20$, $\lambda = 1.0$ and $\kappa = 0.11$

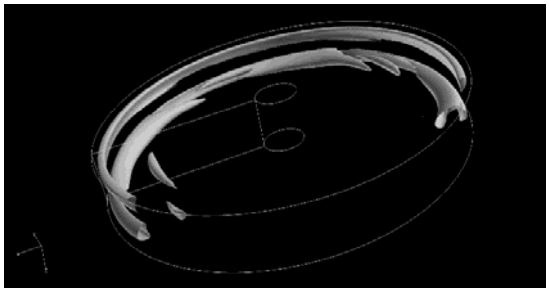

(a) $Q = 3.20$

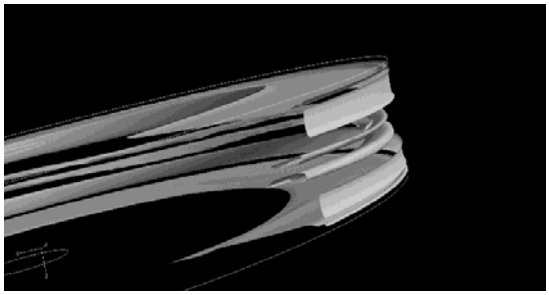

(b) $|\zeta_\theta| = 4.50$

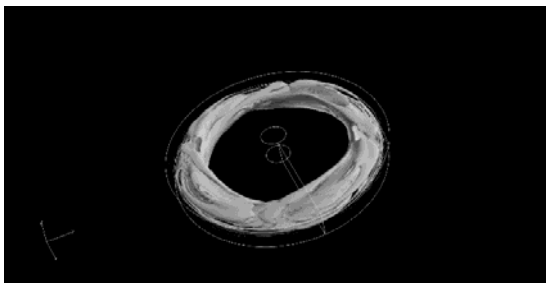

(c) $|\zeta_z| = 0.30$

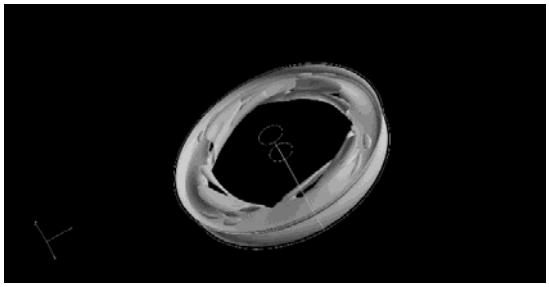

(d) $\zeta_z = 0$

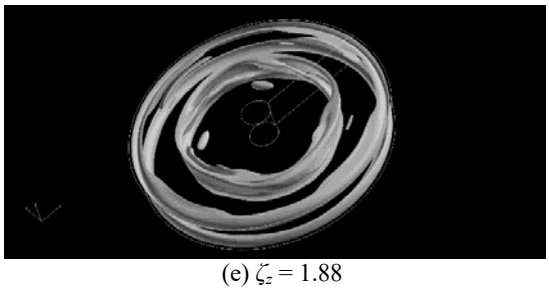

(e) $\zeta_z = 1.88$

Fig. 12 Iso surfaces at an instant in CSM 4 and TVM 2B at $Re = 5.4\times10^3$, $\delta = 0.25$, $\lambda = 1.0$ and $\kappa = 0.11$

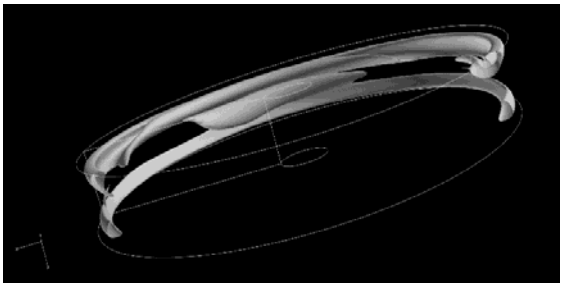

(a) $Q = 2.20$

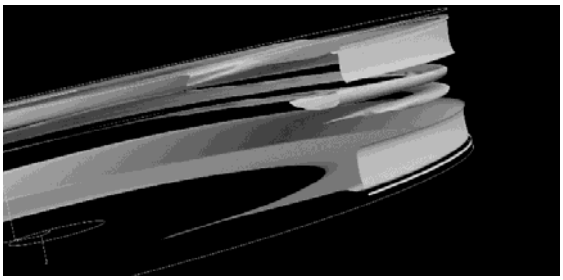

(b) $|\zeta_\theta| = 3.50$

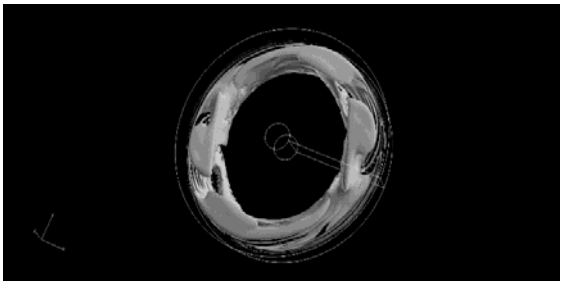

(c) $\zeta_z| = 0.20$

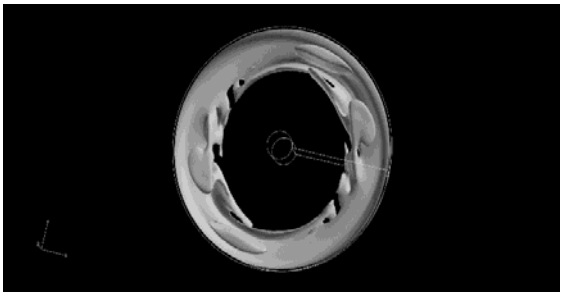

(d) $\zeta_z = 0$

(e) $\zeta_z = 1.87$

Fig. 13 Iso surfaces at an instant in CSM 2 and TVM 2B at $Re = 4.1\times10^3$, $\delta = 0.30$, $\lambda = 1.0$ and $\kappa = 0.11$

pair of the torus vortices characterized by *the shift-and-reflect symmetry* is observed in panel (b) and an almost circular central core in the rigid rotation with disk is found in panel (e).

Fourthly, Fig. 10 exhibits the flow at $Re = 8.2\times10^3$, $\delta = 0.15$, $\lambda = 1.0$ and $\kappa = 0.11$. The flow is in CSM 5 and TVM 1B. Panel (a) well correspond to the flow with the turbulent fluctuation but including one dominant periodicity. The dominant periodicity appearing in Fig. 10(a) seems to be related with the shift-and-reflect symmetry, as well as Fig. 9(a). In Fig. 10(b), the symmetric pair of the torus vortices in Fig. 9(a) are not clear but rather complicated. However, azimuthally- and time-averaged spatial sizes of the torus vorticities in Fig. 10(b) are almost the same each other. Besides, an almost hexagonal central core in the rigid rotation with disks is found in panel (e).

Finally, Figs. 11-13 show the flows in CSM 5 and TVM 2B, CSM 4 and TVM 2B, and CSM 2 and TVM 2B, respectively. Panel (a) well correspond to the flows with a periodic and slightly turbulent fluctuation. It seems difficult to find out the correlation between the periodicity and the shift-and-reflect symmetry in panel (a). As well as Fig. 8, a non-symmetric pair of the torus vortices are observed in panel (b). However, the torus vortices are not clear but rather complicated. An almost-pentagonal, almost-square and almost oval central core with slightly-complicated boundaries are found in Figs. 11(e), 12(e) and 13(e), respectively.

Conclusion

We have considered the flow between the co-rotating disks where the disks which rotate co-axially in the same direction at the same angular velocity and there is a narrow gap enclosed by a stationary shroud at their circumferences. The flow often accompanies azimuthally-fluctuating instabilities: non-axisymmetric secondary flows nears the shroud. In the present study, we experimentally and numerically research the flow in torus-vortex modes TVMs, in addition to core-shape modes CSMs. In experiments, we have visualized the midplane (r-θ plane) and the meridional plane (r-z plane) between co-rotating disks by using a high-speed video camera and a YAG laser to carry out particle-image-velocimetry (PIV) analyses. Based on such PIV results, the torus-vortex modes and the core-shape modes are defined. In numerical analysis which shows good agreement with experimental results, we have reveal the details of flow structure in every mode. The obtain stability diagram of the TVMs are compared with that of the CSMs. The result suggests the complexity of relation between TVMs and CSMs. By numerical calculations, the authors have revealed the details of diverse flow structures in those modes.

The relations between the flow structures of the TVMs and the CSMs still remain unclear and have an open problem. Further studies are required to understand the precise relations.

TSF0025

References

[1] Schlichtuig, H., 1979. *Boundary-Layer Theory, 7th edition,* MacGrow-Hill, New York, 647 – 652.

[2] Karman, T. von, 1921, Uber laminare and turbulente reibung. *Z. Ang. Math. Mech.*, **1**, 1325 – 1336.

[3] Cochran, W. G., 1934, The flow due to a rotating disk. *Proc. Cambridge Philos. Soc.*, **10**, 465 – 491.

[4] Batchelor, G. K., 1951, Note on a class of solutions of the Navier-Stokes equations representing steady rotationally-symmetric flow. *Quarterly J. of Mech. And Appl. Math.*, **4**, 29 – 41.

[5] Stewartoson, K., 1953, On the flow between two rotating coaxial disks. *Proc. Cambridge Phil. Soc.*, **49,** 333 – 341.

[6] Zandbergen, P. J. and Dijkstra, D., 1987, Von Karman swirling flows. *Ann. Rev. Fluid Mech.*, **14**, 465 – 491.

[7] Soo, S. L., 1958, Laminar flow over an enclosed rotating disk. *Trans. ASME*, **80**, 287 – 296.

[8] Maroti, L. A., Deak, G. and Kreith, F., 1960, Flow phenomena of partially enclosed rotating disks. *ASME J. of Basic Engineering.*, **82**, 539 – 552.

[9] Daily, J. W. and Nece, R. E., 1960, Chamber dimension effects on induced flow and frictional resistance of enclosed rotating disks. *ASME J. of Basic Eng.,* **82**, 217 – 232.

[10] Rice, W., 1963, An analytical and experimental investigation of multiple disk pumps and compressors. *ASME J. of Eng. for Power*, **85**, 191 – 200.

[11] Haisnger, S. H. and Kerhrt, L. G., 1963, Investigation of a shaer-force pump. *ASME J. of Eng. for Power*, **85**, 201 – 212.

[12] Stenning, A. H., 1956, Stall propagation in axial compressors. *NACA TN*, **3580**.

[13] Emmons, H. W., Kronauer, R. E. and Rocket, J.A., 1959, A survey of stall propagation-experimental and theory. *ASME J. of Basic Eng.*, **81**, 409 – 416.

[14] Jansen, W., 1964, Rotating stall in a radial vaneless diffuser. *ASME J. of Basic Eng.*, **86**, 750 – 758.

[15] Ohuchida, S., Kawakubo, T. and Tamaki, H., Experimental study of rotating stall in vaneless diffuser of a centrifugal compressor, Proceedings of the ASME Turbo Expo, 6C(2013), pp. 1 – 8.

[16] Lennemann, E., 1974, Aerodynamic aspects of disk files. *IBM J. Res. Develop.*, **18**, 480 – 488.

[17] Abrahamson, S. D., Eaton, J. K. and Koga, D. J., 1989, The flow between shrouded corotating disks. *Physics of Fluids A*, **1**, 241 – 251.

[18] Schuler, C. A., Usry, W. R., Humphrey, J. A. C. and Greif, R., 1990, On the flow in the unobstructed space between shrouded corotating disks. *Physics of Fluids A*, **2**, 1760 – 1770.

[19] Funaki, J and Yano H., 1992, The gap flow between coaxial rotating disks. flow, 10, 274-280.

[20] Funaki, J.,Takizawa, K., Hirata, K. and Yano H., 1995, Flow modes in gap between coaxial rotating disks. *Transactions of the Japan Society of Mechanical Engineers, Series B*, **94**, 2924 – 2928 (in Japanese).

[21] Humphrey, J. A. C., Schuler, C. A. and Webster, D. R., 1995, Unsteady laminar flow between a pair of disks corotating in a fixed cylindrical enclosure, *Physics of Fluids*, **7**, 1225 – 1240.

[22] Herrero, M. A. S. J., Giralt, F. and Humphrey, J. A. C., 1999, Influence of the geometry on the structure of the flow between a pair of corotating disks. *Physics of Fluids*, **11**, 88–96.

[23] Randriamapianina, A., Schiestel, R. and Wilson, M., 2001, Spatio-temporal behaviour in an enclosed corotating disk pair. *J. Fluid Mech.*, **434**, 39 – 64

[24] Hirata, K., Funaki, J., Nishida, Y., Honma, S., Yoshida, H. and Furue, M., 2006, On selection of flow modes between rotating disks. *Transactions of the Japan Society of Mechanical Engineers, Series B*, **72**, 3066 – 3073 (in Japanese).

[25] Hirata, K., Sakamoto, A., Kitagawa, A., Uno, T. and Funaki, J., 2011, On the influence of hub upon flow between co-rotating disks. *Transactions of the JSME, Series B*, **77**, 1920 – 1932 (in Japanese).

[26] Washizu, T., Lubisch, F. and Obi, S., 2013, LES study of flow between shrouded co-rotating disks. *Flow, Turbulence and Combustion*, **91**, 607-621.

[27] Arimitsu, M., Chiba, T., Tanigawa, H., Funaki, J. and Hirata, K., 2013, Visualisation on axialy cross-axial sections of gap flow between co-rotating disks. *Proceedings of the 4th Asian Symposium of Computational Heat Transfer and Fluid Flow*, Paper No. ASCHT0072-T01-1, 1 – 10.

[28] Hirata, K., Chiba, T., Arimitsu, M., Tsugawa, S., Watanabe, T., Maeda, T. and Tanigawa, H., 2015, PIV measurement and numerical analysis of diverse flows between co-rotating disks in casing. , AICFM13, 1-7.

[29] Welch, J. E., Harlow, F. H., Shannon, J. P. and Daly, B. J., 1965, The MAC method, a computing technique for solving viscous, incompressible transient fluid-flow problems involving free surface. *Nuclear Science Abstracts*, 1 – 146.